

Use of mobile phone sensing data to estimate residence and mobility times in urban patches during the COVID-19 epidemic: The case of the 2020 outbreak in Hermosillo, Mexico

L. Leticia Ramírez-Ramírez ^{*1}, José A. Montoya ^{†2}, Jesús F. Espinoza ³,
Chahak Mehta ⁴, Albert Orwa Akuno ⁵, and Tan Bui-Thanh ⁶

¹*Centro de Investigación en Matemáticas A.C., Mexico*

²*Universidad de Sonora, Mexico*

³*Universidad de Sonora, Mexico*

⁴*University of Texas at Austin, USA*

⁵*Centro de Investigación en Matemáticas A.C., Mexico*

⁶*University of Texas at Austin, USA*

October 30, 2022

Abstract

It is often necessary to introduce the main characteristics of population mobility dynamics to model critical social phenomena such as the economy, violence, transmission of information, or infectious diseases. In this work, we focus on modeling and inferring urban population mobility using the geospatial data of its inhabitants. The objective is to estimate mobility and times inhabitants spend in the areas of interest, such as zip codes and census geographical areas. The proposed method uses the Brownian bridge model for animal movement in ecology. We illustrate its possible applications using mobile phone GPS data in 2020 from the city of Hermosillo, Sonora, in Mexico. We incorporate the estimated residence-mobility matrix into a multi-patch compartmental SEIR model to assess the effect of mobility changes due to governmental interventions.

Keywords: Brownian Bridges; urban mobility; mobile phone data; epidemic modeling.

^{*}Electronic address: leticia.ramirez@cimat.mx

[†]Electronic address: montoya@mat.uson.mx; Corresponding author

1 Introduction

Critical social phenomena such as violence, economy, transmission of information, culture and infectious diseases are naturally linked to human mobility and as we are experiencing a constant increase in global and regional connectivity, it is imperative improving our understanding of mobility patterns to develop more realistic mathematical models [26, 42, 51]. Detailed human mobility records of a particular regional population can be obtained from mobile phone records [48] and such information can be used to predict future user's locations, validate human mobility models [36], study the role of human mobility and estimate the main characteristics of social networks [55], among others. Indeed, the desire to understand and predict how human population moves in real world has been one of the main goals for data collected by mobile phone service providers [40]. The diversity of the application of the study of human mobility cannot be over-emphasized. For instance, in the area of transportation, the study of human mobility can be used as a guide to the optimization of road networks and public transport systems thereby leading to efficient city planning and engineering [40]. The study of human mobility is also important in the provision of humanitarian relief services after the occurrence of natural large-scale disasters like earthquakes. A particular research work in this area is by [30] who studied the predictability of human displacement and mobility, long-term reconstruction of the society and effective humanitarian relief operations after the Haiti 2010 earthquake. In the health sector, human mobility data has become an integral part of policy formulation by public health officials as regards to the control and ending the spread of infectious diseases [10, 16, 45, 57, 44]. Analysis of real world social problems through social networks has been made possible by social graphs induced by mobile communications. For instance, [8, 17, 35, 52] studied discovery of meaningful community structure through use of connected graphs.

The heterogeneous human interactions can significantly impact the dynamics we study. In epidemiology, traditional mass-action compartmental models have proven their usefulness for different infectious agents to model infection dynamics at a regional level. However, for several diseases, it is crucial to consider the structure of sub-populations (patches) and their heterogeneous contacts, that are usually induced by the spatial configuration and mobility.

To introduce heterogeneous human contacts, the epidemics in networks model (or reaction-diffusion models on meta population networks) have played an essential role in journals with a physics focus [13, 12, 54, 47]. Nevertheless, the model inference, fit or selection, uses highly computing-intensive numeric methods such as MCMC or particle filtering based on Monte Carlo simulations. Unfortunately, the scaling of these methods makes them prohibitive when considering medium to larger size populations.

This paper focuses on estimating the information used in the class of patchy epidemic models [6, 1] that fall in an intermediate complexity between mass-action and networks

models. These models introduce population heterogeneities at the level of sub-populations and can include the within and between contact patterns induced by mobility.

Several epidemic models have proposed the introduction of regional mobility patterns [3, 7, 6, 16, 59, 31] for human-to-human infectious diseases [34, 5, 27] or vector-borne diseases [29, 14, 2, 32]. These can incorporate mobility with an emphasis on a regional scale, which is critical in the increasing number of cases at the beginning of the outbreak [33]. However, we want to evaluate the mobility at metropolitan area scale since most of these movements occur in the context of the day-to-day existence of the 55% of the world's population that lives in cities [60, 53].

Several authors identify and model mobility patterns using diverse sources, spanning from official information (surveys, census) to GPS, social media and online data [4]. While official data and social networks can provide information on mobility in a large region (between states or countries), we require more detailed information (spatial and time-wise) to describe mobility in a metropolitan area.

For decades, the animal movement has been a matter of interest, and the data typically considered comes from attached or implanted devices. This technology can generate detailed data sets of movement patterns. However, until recently, in the human case, geolocated smartphones have been used as an effective tracking device voluntarily carried by billions of people. The big data generated by these devices describe human mobility and behavior both with unprecedented high spatial resolution and high frequency. These characteristics allow studying the human main traveling patterns on a smaller time-space scale [37, 42, 46, 19]. Without a doubt, mobile phones represent a very valuable source of information for studying people's behaviors, for environmental monitoring, transportation, social services, businesses [18] and have untapped potential to serve as tools for public health.

Although the potential use of data originating from cellular networks has been identified for some years, the analyzes are usually focused on estimating population sizes in the areas of interest, type of activities in the city, hotspot, as well as characteristics of mobility patterns described by contact networks [9] or by metrics [23]. All these are derived directly from the reported GPS records and aggregated in time intervals.

In the context of epidemiological models, some types of movements that have been of interest are those that tend to be more regular, such as commuting between two regions [50]. These movements are usually estimated by the frequency of GPS reports in each area. In more theoretical approaches, the authors assume a specific model for the human mobility from one region to another, such as adjacency and gravity [26, 4] or the impact of the mobility, according to the model, is illustrated under different mobility scenarios [51].

As these epidemic models consider individuals' commuting, the mobility estimation reduces to inferring the percentage of individuals for each pair of residence and destination regions. However, epidemiological models, such as [6, 1], regard mobility not

only as commuting between two areas but also as the different temporal contacts that individuals have with individuals on the routes to various destinations during the day. These other epidemiological models then use the information on the origin (residence) and the proportion of time individuals spend in each region (including its own). We propose estimating this residence-mobility matrix with a model that takes into consideration the individuals' sequence of GPS reports ('pings') and the stochastic variation from the path between consecutive locations.

The objective is to identify the individual residency area and statistically estimate the average times inhabitants spend in each of the n areas of interest in the city (such as zip codes and census geographical areas -AGEBs-). We produce a $n \times n$ non-negative matrix that describes the proportion of time that each individual with a specific residence, expect to spend in each area. The proposed method is based on Brownian bridge process used for animal movement in ecology. This allows us to estimate the individual location at any time between pings. We applied the proposed method to data from the city of Hermosillo, Mexico, during the COVID-19 pandemic.

The remainder of this paper is organized as follows: Section 2 presents the mobile phone sensing data and its required pre-processing. In Section 3 we describe the data filtering and proposed methods for residence selection, prior to the residence-mobility matrix estimation. In Section 4 we present the Brownian bridge models used and describe the numerical procedures executed. Section 5 shows the resulting residence-mobility matrix estimates for two times periods (from 2020-09-15 to 2020-10-15, and from 2020-10-16 to 2020-11-15). The state of Sonora, according to the implemented epidemic traffic light, moved from yellow to orange after the second period. In Section 6 we illustrate its applicability by implementing it on a patchy epidemic model for Hermosillo. Finally, in Section 7 we discuss the results and future work.

2 Mobile phone sensing data

Mobile phone tracking is a process for identifying the location of a mobile phone based on diverse technologies and methods that include multilateration (triangulation) of radio signals and using a global navigation satellite system (GNSS, GPS -Global Positioning System- in North America). The first technology uses the constant roaming radio signals that a mobile phone emits and may be picked up by three or more stationary cell towers enabling the triangulation to work. The location of a mobile device is estimated using the coordinates (longitude, latitude) of nearby cell towers and the estimated distance of the device from each tower (either using signal strength or the time delay that a signal takes to return to the towers from the phone, for example). In contrast, GNSS allows for a high precision localization (within a few centimeters to meters) of signals that operate independently of any telephonic or internet reception. The Global Positioning System

(GPS) technology is a satellite-based system operated by the United States Space Force that provides geolocation and time information to a GPS receiver anywhere on the Earth, where there is an unobstructed line of sight to at least four GPS satellites. A mobile phone ‘ping’ is the process of sending a signal to a particular mobile phone and this responding with the request data to determine its location by utilizing its GPS location capabilities. The multilateration and GNSS/GPS pings correspond to analog and digital process, respectively.

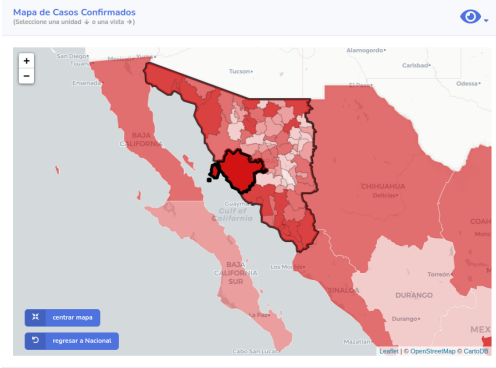
The data that we use in this research corresponds to GPS pings collected by mobile service providers when users access specific (but undisclosed) apps for which they have granted permission to access their location information.

On September 14, 2020, in the city of Hermosillo, Sonora, Mexico, the University of Sonora signed an agreement with the company Lumex Consultores S.C., with the aim of providing statistical consulting services for estimating characteristics of the population of Hermosillo, related to COVID-19 cases. This agreement allowed access, under conditions of confidentiality that allow us to make public scientific results, to GPS data from mobile phone reports for an area that covers the city of Hermosillo.

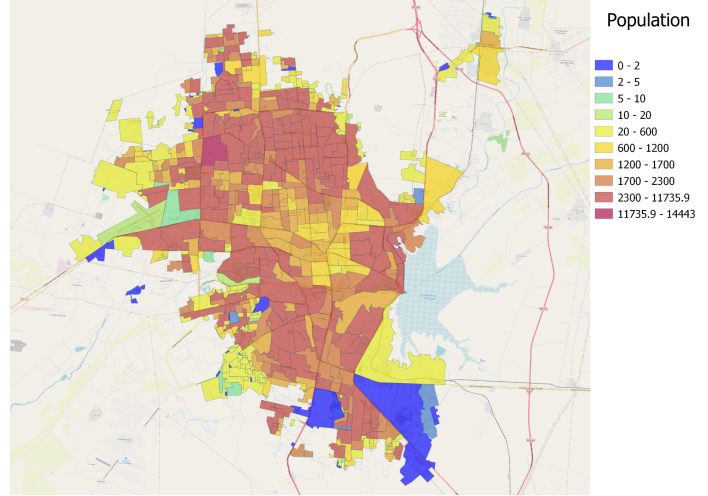
The raw data, acquired by Lumex Consultores, was weekly stored in a daily-partitioned table in BigQuery (a Google Cloud service). Through the API service and SQL queries, we could download specific sub-data bases as well as the whole database, in order to do the data wrangling prior to the analysis.

The city of Hermosillo is in the state of Sonora at the Mexico northwest and has an area of 169.55 km². It is the capital of the state and it is located 280 km south of the border with the United States and about 110 km from the coast of the Gulf of California. More precisely, it is located at the 29°05' parallel of north latitude and the 110°57' meridian of west longitude from Greenwich (Figure 1A). The Population and Housing Census¹, carried out by the National Institute of Statistics and Geography (INEGI) in 2020, reports a population of 2,944,840 in the state of Sonora. The municipality with the largest population in the state of Sonora corresponds to the city of Hermosillo, with a total population of 936,263.

¹Census 2020, <https://www.inegi.org.mx/programas/ccpv/2020/>



(A) Hermosillo municipality, Sonora. Mexico.



(B) Hermosillo city and its AGEB's.

Figure 1: Hermosillo and its AGEB's. Source: <https://datos.covid-19.conacyt.mx/>, <https://www.inegi.org.mx/app/biblioteca/ficha.html?upc=889463807469>.

The local time zone in Hermosillo corresponds to UTC-07:00 throughout the year, as this state, as well as Quintana Roo, do not switch to the national summertime, that in 2020 was from April 5 to October 25.

2.1 The variables of mobility data

The mobility data used in this work consists of 80,582,452 records, which contain the variables in Table 1 that we describe afterwards.

Variable	Description
id_adv	mobile phone's ID (unique to each device)
timestamp	Ping date and time
lat	Ping's Latitude
lon	Ping's Longitude
gender	Declared gender by user
age	Declared age

Table 1: Variables in mobile phone sensing dataset.

id_adv It is a unique alphanumeric id, associated with each device (mobile phone). In the database there exist 306,963 such id's. Every time that a device uses some specific app, with GPS localization capabilities allowed, that is, makes a ping, then a new record is added to the database. The number of pings per device goes from 1 to 18,297.

However, 96.41% of such devices have at most 1,000 records on the full database.

timestamp Corresponds to a sequence of characters in format YYYY-MM-DD hh:mm:ss UTC pointing out the day and time which a device made a ping. All such timestamps belong to the timeframe from 00:00:00 on the 18th of September 2020 to 23:59:59 on December 13, 2020, in Universal Time Coordinated (UTC). However, to estimate the urban mobility, to determine various sanity checks and in determining the patch of residence for an individual, for the city of Hermosillo, according to the criteria that will be indicated later (Section 3.2), we transform the timestamp variable to the local time zone. So the local dates and times on which each of the mobility data observations were recorded are between 15:00, 2020-09-17 and 15:00, 2020-12-13.

lat, lon Two columns with numerical values to indicate the position (latitude and longitude coordinates) where the device made ping. We transform this coordinate data to cartesian coordinates using the UTM (Mercator) projection. This transformation was done using the `geopandas` library in Python and it allows us to calculate distances between the GPS data points. The data recorded in the database takes values from 28.975325354058949 to 29.196006913613104 for the latitude and from -111.10024483411226 to -110.8457 for the longitude.

gender String of characters with values: `male` or `female`. This variable is set up by the device owner.

age Range of numerical values at which belongs the age of the user. This variable is set up by the user and the values recorded in the database are: `> 55`, `41 – 55`, `26 – 40`, `18 – 25` and `12 – 17`.

The last variable is not considered in this work. Next we describe the temporal and spatial characteristics of the data.

Periodic behavior due to daily commuting and activities, such as school, rush hours, lunch, and night-time, characterize population mobility in urban areas. These aspects might also change by type of day (weekday or weekend), and the availability of local transport systems [19]. In Figure 2 we present the count relative frequency of timestamp by weekday and hour of the day during the study period. This figure shows a high degree of temporal regularity and patterns are consistent with people’s activity schedules in the city. For example, activity decreases at dawn and increases in hours associated with work and leisure activities. We can also observe that weekend activities can produce very different curves.

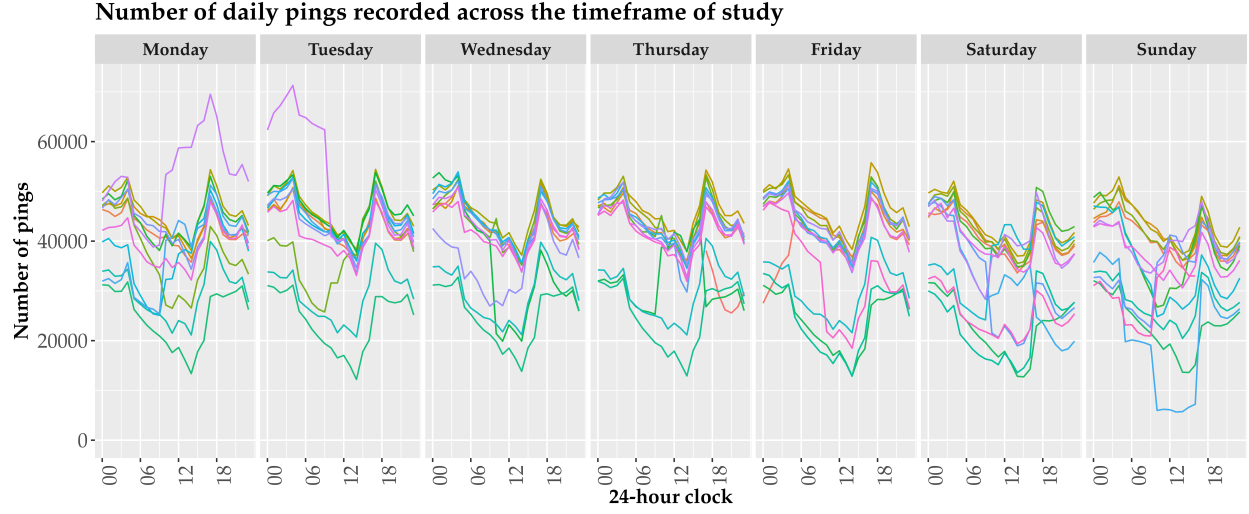


Figure 2: Number of pings by weekday and hour.

Figure 3 shows the bivariate normal kernel density estimate for traveled distance between consecutive pings and travel time (in a logarithmic scale for proper visualization) using all pings recorded during the study period from a sample of 10,000 id's. This graph was generated using MASS package in R and selecting kde2d's default parameters. The vertical dotted lines mark the corresponding time scale in minutes and/or hours. Similarly, the horizontal dotted lines mark the corresponding distances traveled in meters and/or kilometers. From the figure, we observe that most consecutive pings are at intervals between 2 and 30 minutes. These are divided into those where people move only few meters (likely walking or in a workspace) and those where they move between 30 and 500 meters (likely in a vehicle). At the top right, a third, less important group spends between 2 and 40 hours between pings but moves 500 to 10,000 meters.

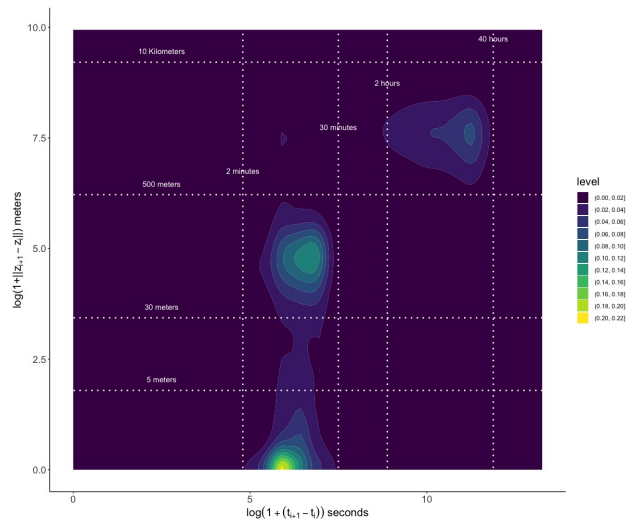


Figure 3: Kernel density of distance and consecutive pings.

To carry out censuses and surveys, it is necessary to define, in the geographical area, the study areas. Such units are called Geostatistical Areas and in Mexico these are: State (AGEE), Municipal (AGEM) and Basic (AGEB). The latter is the smallest and fundamental geographical area and may be urban or rural. Urban AGEB's delimit a part or the total of a locality of 2500 inhabitants or more. In larger towns and cities, these AGEBs generally groups 25 to 50 blocks.

In the case of the city of Hermosillo, there are 587 urban AGEB's whose population sizes are illustrated in Figure 1B.

3 Data filtering and residence selection

In this section, we show how we filter the mobility phone data by the number of pings per id (device id) in a timeframe, to properly carry out the computation of the Brownian bridges (Section 4). We also propose a criterion for the residence selection for any id after filtering. We have chosen three periods, each divided into two parts, to estimate the mobility patterns. Table 2 presents these timeframes.

Abreviation	Full name	Start date	End date
FP_FP	First Period - First Part	2020-09-21	2020-10-04
FP_SP	First Period - Second Part	2020-10-26	2020-11-08
SP_FP	Second Period - First Part	2020-09-21	2020-10-04
SP_SP	Second Period - Second Part	2020-11-02	2020-11-15
TP_FP	Third Period - First Part	2020-09-21	2020-10-11
TP_SP	Third Period - Second Part	2020-10-12	2020-11-01

Table 2: Periods within which the mobility matrices were estimated.

The main reason for selecting the periods under study was that they would include the yellow phase of the COVID-19, determined by the Secretary of Health of the State of Sonora. Figure 4 indicates, using colors (top of the graph), the behavior of the status of COVID-19 for Hermosillo between the second half of 2020 and the beginning of 2021. It also shows the number of confirmed cases per day, a moving average to visualize the general epidemic pattern, and two vertical lines that indicate the time window for which mobility data is available. Based on this figure, it is easy to verify that all selected periods are not only in the yellow phase of the COVID-19. They include the later stage of the first wave of COVID-19 and a period before the start of the second wave of COVID-19 cases in Hermosillo. Furthermore, the second part of each period shows no indication that the confirmed cases of COVID-19 have an accelerated increase. In fact, the moving average indicates a slight downward slope between 2020-09-21 and 2020-11-15, dates that cover our selected periods. Thus, in terms of confirmed cases, the second part of each period does

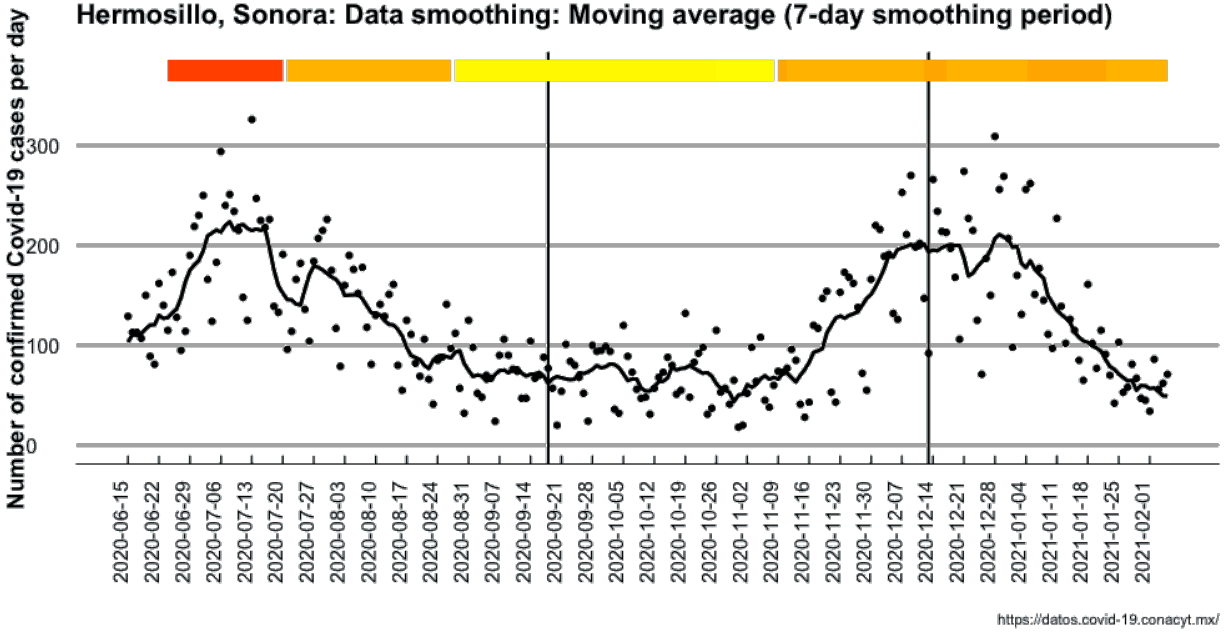


Figure 4: Daily confirmed cases of Covid-19 in Hermosillo, Sonora, in the timeframe of study.

not herald the future presence of the second wave of COVID-19 cases. Concerning urban mobility, we hypothesized that the second part of each period could be associated with an increase in the mobility of people in the city, as they include the dates of the traditional day of the dead and Halloween. Both festivities are celebrated effusively in cemeteries, markets, and streets.

3.1 Data selection

The original mobility data in the database consists of 80,582,452 pings that register the timestamp of 306,963 devices (ids). However, to proceed with the estimation, we filter them to ensure a minimum of pings per device in each part.

Table 3 contains the number of ids that in any of the two parts, of the corresponding period, report at least 5, 11, 15, or 21 pings. The table also shows its magnitude as the percentage of the number of ids with at least one ping in any of both parts.

If we are interested in comparing the change of individual mobility patterns, we select the ids with at least 5, 11, 15, or 21 pings in both parts of each period. Naturally, the number of ids under this criterion decrease as Table 4 presents. The percentage is now with respect to the number of ids with at least one ping for each parts.

To perform the Brownian bridges' computation, as described in the next section, we filter the mobile phone database for each period by dropping the ids with less than 10 pings

Period	+5 pings	+11 pings	+15 pings	+21 pings
First	217396 (88.74%)	153117 (62.5%)	85742 (35%)	44859 (18.31%)
Second	226174 (89.05%)	154374 (60.78%)	89831 (35.37%)	46456 (18.29%)
Third	186448 (88.12%)	128915 (60.93%)	68485 (32.37%)	32416 (15.32%)

Table 3: Ids distribution per period.

Period	+5 pings	+11 pings	+15 pings	+21 pings
First	125608 (82.13%)	79013 (51.66%)	40278 (26.34%)	17105 (11.18%)
Second	123748 (81.7%)	74034 (48.88%)	40086 (26.47%)	17310 (11.43%)
Third	126268 (82.8%)	76360 (50.07%)	37952 (24.89%)	15324 (10.05%)

Table 4: Ids distribution per period present in both parts.

weekly. That is, for each period and each part, we keep ids with at least 11 pings in any of the two parts. Table 5 shows the number of ids selected for each period/part and used to compute the residence time matrices through the Brownian bridges.

Period	Part	+11 pings
First	First	108252
	Second	123878
Second	First	108252
	Second	120156
Third	First	102091
	Second	103184

Table 5: Number of ids selected for each period/part.

Hence, the ‘+11 pings’ column in Table 3 is obtained from the union (as sets) of the ids in the first and the second part of each period in Table 5. Also, the corresponding column in Table 4 is given by the intersection of the ids in both parts for each period in Table 5.

The population in Hermosillo city is about 936,263 inhabitants, then the number of ids selected to represent the mobility is above 10.9% for any period/part.

3.2 Residence selection

Since we are interested in describing mobility at the AGEb level, it is necessary to identify the AGEb to which each ping’s location belongs. For this, it is essential to transform the

latitude and longitude data to the UTM coordinate system and identify the AGEb to which it corresponds. We do this using the AGEb's official polygon information.

Now, as we also want to describe the mobility patterns for all individuals that live in each AGEb, and this information is not available for each id, it is necessary to assign each id to an AGEb as a residence using the very same database. To determine the AGEb that users of each device live, we use the following heuristic (described in Algorithm 1), that combines criteria of frequency, timeframes, and AGEb's population size.

Algorithm 1 Find the residence of all individuals

```

for each individual  $i$  do
   $s1 \leftarrow$  AGEbs with maximum GPS data points
   $s2 \leftarrow$  AGEbs with maximum GPS data points between 10 p.m. and 6 a.m.
   $f = s1 \cap s2$ 
  if  $\text{len}(f)$  is 1 then
     $\text{residence}_i \leftarrow f$ 
  else
     $\text{residence}_i \leftarrow f_i$  where  $i$  is selected randomly weighted by population of  $f_i$ 
  end if
end for

```

4 Statistical modeling, inference and computational aspects

One of the first papers that discussed urban analysis using data originated from mobile phones was [43] and was followed by works that highlighted possibilities of real-time visualization and monitoring of displacements in cities. In general terms, now we can distinguish models of human mobility aimed at reproducing individual mobility patterns or general population flows [4].

The residency-mobility matrix that we estimate can be viewed as a general population flow that describe the mobility patterns for individuals who inhabit each AGEb, but it is based on individual mobility modelling as we first estimate individual paths between consecutive pings. In the next sections we describe the model and the inference we propose.

4.1 The Brownian bridge model

Suppose that $Z_{rj}(t)$ represents the position of the j -th resident from r -th patch along the xy plane at time t . We assume that N_r is the resident population size in patch r , and we denote by R the the number of patches considered. Let $\{Z_{rj(1)}, t_{rj(1)}\}, \{Z_{rj(2)}, t_{rj(2)}\},$

$\dots, \{z_{rj(n_{rj})}, t_{rj(n_{rj})}\}$ be n_{rj} space-time observations collected during the time interval $[0, T_{rj}]$, where $T_{rj} = t_{rj(n)} - t_{rj(1)}$ and $z_{rj(i)}$ is the i -th observed ping location of the j -th resident from r -th patch at time $t_{rj(i)}$. Now let $Z_{rj}^{[k]}(t)$ denote the unobserved position of the j -th resident from r -th patch at time $t \in (t_{rj(k)}, t_{rj(k+1)})$ which undertakes a random walk from positions $z_{rj(k)}$ to $z_{rj(k+1)}$. If a Brownian motion is assumed between these two positions, then $Z_{rj}^{[k]}(t)$ is distributed according to a bivariate normal distribution at time $t \in [t_{rj(k)}, t_{rj(k+1)}]$, with mean vector and covariance matrix given by

$$\mu(t; z_{rj(k)}, z_{rj(k+1)}) = z_{rj(k)} + (z_{rj(k+1)} - z_{rj(k)}) \left(\frac{t - t_{rj(k)}}{t_{rj(k+1)} - t_{rj(k)}} \right), \text{ and}$$

$$\Sigma(t; \sigma_{rj}) = \sigma_{rj}^2 \left[\frac{(t - t_{rj(k)})(t_{rj(k+1)} - t)}{(t_{rj(k+1)} - t_{rj(k)})} \right] \mathbb{I}.$$

Where \mathbb{I} is the 2×2 identity matrix and σ_{rj}^2 is the Brownian motion variance related to the mobility of the j -th resident from r -th patch. Thus, the Brownian bridge process has the property of being normal along a straight line joining the points $z_{rj(k)}$ and $z_{rj(k+1)}$. In addition, the maximum variability is obtained at the middle of the trajectory and the variance equals 0 when $t = 0$ or $t = T_{rj}$. This assumption is adequate when the location reports are precise, but in many applications it is convenient to introduce the uncertainty related to measurement errors. For this, we consider that the starting and ending locations are bivariate normal $N(z_{rj(k)}, \delta^2 \mathbb{I})$ and $N(z_{rj(k+1)}, \delta^2 \mathbb{I})$, where δ^2 is the variance of the location error. Therefore the expected time spent at location z , during $[t_{rj(k)}, t_{rj(k+1)}]$, is

$$h_{rj}^{[k]}(z; \sigma_{rj}, \delta) = \frac{1}{T_{rj}^{[k]}} \int_0^{T_{rj}^{[k]}} \phi\left(z; \mu_{rj}^{[k]}(t), \sigma_{rj}^{[k]}(t; \sigma_{rj}, \delta) \mathbb{I}\right) dt, \quad (1)$$

where

$$\begin{aligned} T_{rj}^{[k]} &= t_{rj(k+1)} - t_{rj(k)}, \\ \mu_{rj}^{[k]}(t) &= z_{rj(k)} + (z_{rj(k+1)} - z_{rj(k)}) \alpha_{rj}^{[k]}(t), \\ \sigma_{rj}^{[k]}(t; \sigma_{rj}, \delta) &= T_{rj}^{[k]} \alpha_{rj}^{[k]}(t) \left(1 - \alpha_{rj}^{[k]}(t)\right) \sigma_{rj}^2 + \left(1 - \alpha_{rj}^{[k]}(t)\right)^2 \delta^2 + \left(\alpha_{rj}^{[k]}(t) \delta\right)^2, \text{ and} \\ \alpha_{rj}^{[k]}(t) &= (t - t_{rj(k)}) / T_{rj}^{[k]}. \end{aligned}$$

Using the $(n_{ri} - 1)$ bridges, we then can estimate the density of the expected occupation time for each individual, as a mixture of the densities (1). That is

$$h_{rj}(z; \sigma_{rj}, \delta) = \sum_{k=1}^{n_{rj}-1} \left(\frac{T_{rj}^{[k]}}{T_{rj}} \right) h_{rj}^{[k]}(z; \sigma_{rj}, \delta). \quad (2)$$

For computing the overall fraction of time spent in a region A (occupation time in A), by individuals from patch r , we average the individual fractions of times in A considering all its patch residents as

$$P_r(A) = \frac{1}{N_r} \sum_{j=1}^{N_r} \int_A h_{rj}(z; \sigma_{rj}, \delta) dz. \quad (3)$$

4.2 Likelihood inference

First, we assume that the variance of the location error δ^2 can be known from the device specifications, while the individual variance σ_{rj} of the mobility of the j -th resident from r -th patch is unknown. We estimate σ_{rj} using the method proposed in [21] (also see [38]). Therefore, we consider the n_{rj} that are odd and estimate the mean based on the independent Brownian bridges for the non-overlapping time intervals

$$\{[t_{rj(k-1)}, t_{rj(k+1)}]\}_{k \in \{2, 4, \dots, n_{rj}-1\}},$$

while regarding the in-between observation times $t_{rj(k)}$ as independent observations from these bridges to estimate σ_{rj} . Thus, $Z_{rj}(t_{rj(k)})$ is a bivariate normal random variable with mean and covariance matrix given by

$$\begin{aligned} \mu(t_{rj(k)}; z_{rj(k-1)}, z_{rj(k+1)}) &= z_{rj(k-1)} + (z_{rj(k+1)} - z_{rj(k-1)})\alpha_{rj(k)}, \\ \Sigma(t_{rj(k)}; \sigma_{rj}) &= [T_{rj(k)}\alpha_{rj(k)}(1 - \alpha_{rj(k)})\sigma_{rj}^2 + (1 - \alpha_{rj(k)})^2\delta^2 + \alpha_{rj(k)}^2\delta^2] \mathbb{I}, \end{aligned}$$

where $T_{rj(k)} = t_{rj(k+1)} - t_{rj(k-1)}$ and $\alpha_{rj(k)} = (t_{rj(k)} - t_{rj(k-1)})/T_{rj(k)}$.

Therefore, the likelihood function of the parameter σ_{rj} can be written as

$$L(\sigma_{rj}) = \prod_{k=2,4,\dots,n_{rj}-1} \phi(z_{rj(k)}; \mu(t_{rj(k)}; z_{rj(k-1)}, z_{rj(k+1)}), \Sigma(t_{rj(k)}; \sigma_{rj})) \quad (4)$$

where again $\phi(\cdot; \mu, \Sigma)$ is the probability density function of a bivariate normal distribution with mean vector μ and covariance variance Σ .

The maximum likelihood estimate for σ_{rj} is the value $\hat{\sigma}_{rj}$ that maximizes $L(\sigma_{rj})$ in (4). Thus for any individual originating from patch r , the estimated probability density function at position z is given by

$$\hat{h}_r^*(z) = \frac{1}{n_r} \sum_{j=1}^{n_r} h_{rj}(z; \hat{\sigma}_{rj}, \delta). \quad (5)$$

Then we can estimate the expected occupation time in A from resident of patch, based on (3), as

$$\hat{P}_r(A) = \int_A \hat{h}_r^*(z) dz = \frac{1}{n_r} \sum_{j=1}^{n_r} \int_A h_{rj}(z; \hat{\sigma}_{rj}, \delta) dz. \quad (6)$$

If the information of the device's location error δ^2 is unknown, we can opt for the BMME extension proposed by [41] based on the joint distribution of $(B_t, Z_{rj}(t_{rj(1)}), \dots, Z_{rj}(t_{rj(n_{rj})}))^\top$ where $Z_{rj}(t_{rj(i)}) = B_{t_{rj(i)}} + \xi_i$, $i = 1, \dots, n_{rj}$, $\{\xi_i\}$ are iid Gaussian variables with mean 0 and variance δ^2 that are also independent of the Brownian motion $\{B_t, t \geq 0\}$.

Since $(B_t, Z_{rj}(t_{rj(1)}), \dots, Z_{rj}(t_{rj(n_{rj})}))^\top$ is a multivariate gaussian vector, then conditional ditribution

$$\Pr(B_t \in dx \mid \mathbf{Z}) \sim \text{MVN}(\mu_{rj}^{[k*]}(t) = \Sigma_{12}\Sigma_Z^{-1}\mathbf{Z}, \sigma_{rj}^{[k*]}(t) = \sigma_{rj}^2 t - \Sigma_{12}\Sigma_Z^{-1}\Sigma_{12}^\top)$$

where $\mathbf{Z} = (Z_{rj}(t_{rj(1)}), \dots, Z_{rj}(t_{rj(n_{rj})}))$,

$$[\Sigma_Z]_{i,s} = \text{Cov}(Z_{rj}(t_{rj(i)}), Z_{rj}(t_{rj(s)})) = \begin{cases} \sigma_{rj}^2 t_{rj(i)} + \delta^2 & \text{if } i = s \\ \sigma_{rj}^2 \min\{t_{rj(i)}, t_{rj(s)}\} & \text{if } i \neq s \end{cases},$$

and $\Sigma_{12} = \sigma_{rj}^2 [\min(t, t_{rj(1)}), \dots, \min(t, t_{rj(n_{rj})})]$.

Then the density of the expected occupation time for each individual (2) corresponds, under BMME, to

$$h_{rj}(z) = \sum_{k=1}^{n_{rj}-1} \left(\frac{T_{rj}^{[k]}}{T_{rj}} \right) \left[\frac{1}{T_{rj}^{[k]}} \int_{t_{rj(k)}}^{t_{rj(k+1)}} \phi(z; \mu_{rj}^{[k*]}(t), \sigma_{rj}^{[k*]}(t)) dt \right]. \quad (7)$$

The downside of introducing one extra parameter to infer is outweighed by the advantage of using all the data at the same time to estimate all parameters and the fact that this inference is not computationally more expensive to implement. Once the maximum likelihood estimates are obtained we obtain the expected occupation time in region A as in (6).

We estimate the residence-mobility matrices for each Period and Part as in Table 2. For each period, We compare the estimated matrices using some of the most important distances. Table 6 presents the Euclidean, Manhattan and Minkowsky distances and we observe that under all metrics, the matrices for the First Period are the most different.

	Euclidean	Manhattan	Minkoswky(p = 3)
First Period	3.0168	220.3977	1.1631
Second Period	2.3036	196.1594	0.8797
Third Period	2.0883	182.3302	0.7590

Table 6: Matrices distances for estimated matrices in each period.

The first part corresponds to the early period of low number of cases (See Figure 4) while the second part is just prior to a new wave in the epidemic curve. The festivities of “Dia de los muertos” in Mexico fall within the second part promoting the urban mobility that could be an important factor for the following wave. Next, We explore the effect of the residence-mobility in the epidemic outbreak.

5 The multi-patch epidemic model with mobility and residency

Increasing connectedness of world countries and cities either through road, rail or air transport has led the world to become a global village over time. For illustration purposes

in this article, we focus on the role of human mobility on epidemic spread. Remaining at the forefront as issues to be addressed by epidemiologists are the epidemiological challenges threatening the economic and social stability of many world regions, particularly, those dependent on human mobility and trade [39]. The ability of human population to live, travel and/or trade almost anywhere across the globe has increasingly and continuously shaped and reshaped the global social and economic activities. Indeed, perceived or real economic and social risks may be some of the factors driving and shaping mobility behaviour of individuals within and between cities or patches [10]. Consequently, it has become increasingly important to understand and quantify the interaction patterns of human populations, especially in the face of a pandemic as such has a direct effect on the economic and social fabric of a society.

The effects of such human interaction patterns in the presence of an infectious disease can be understood and unraveled through meta-population-multi-patched models [15, 20, 22]. The main intention of understanding such human mobility patterns in the face of a pandemic is to formulate a combination of various measures, such as mobility restrictions, in order to control the spread of the disease as it has been confirmed that an infectious disease can swiftly be propagated by global and individual dynamics of activities and mobility [11, 56, 58]. In fact, [25] posits that the spread of an epidemic largely depends on the likelihood of infection and individual human interaction with mobility networks playing a vital role in aiding temporal and spatial dynamics of disease evolution within human population. This observation was further affirmed by [49] who compared the evolution of an infectious disease in a local and global scale to a reaction-diffusion process with the reaction stage corresponding to the interaction of the hosts of the pathogen with the susceptible group and the diffusion stage corresponding to the movement or mobility of the infected group, spatially propagating the pathogen.

In this research, we apply the estimated mobility-residence-time in an epidemic model and assess the effect of different matrices estimated for different time periods. It is against this background that we apply and implement the estimated residence times and the mobility parameters α_i using our methodology to a meta-population multi-patched SEIRS compartmental model with mobility and residency. This model was proposed by [1] and we refer the reader to this article in order to have a full knowledge and the intuition behind the formulation and the derivation of the model.

The considered epidemic model is:

$$\begin{cases} \dot{S}_i &= \Lambda_i - \beta_i(1 - \alpha_i)S_i \frac{(1-\alpha_i)I_i + \sum_{k=1}^n \tilde{p}_{ki}I_k}{(1-\alpha_i)N_i + \sum_{k=1}^n \tilde{p}_{ki}N_k} - \sum_{j=1}^n \left(\beta_j \tilde{p}_{ij} S_i \frac{(1-\alpha_j)I_j + \sum_{k=1}^n \tilde{p}_{kj}I_k}{(1-\alpha_j)N_j + \sum_{k=1}^n \tilde{p}_{kj}N_k} \right) \\ &\quad - \mu_i S_i + \tau_i R_i \\ \dot{E}_i &= \beta_i(1 - \alpha_i)S_i \frac{(1-\alpha_i)I_i + \sum_{k=1}^n \tilde{p}_{ki}I_k}{(1-\alpha_i)N_i + \sum_{k=1}^n \tilde{p}_{ki}N_k} + \sum_{j=1}^n \left(\beta_j \tilde{p}_{ij} S_i \frac{(1-\alpha_j)I_j + \sum_{k=1}^n \tilde{p}_{kj}I_k}{(1-\alpha_j)N_j + \sum_{k=1}^n \tilde{p}_{kj}N_k} \right) \\ &\quad - (\kappa_i + \mu_i)E_i \\ \dot{I}_i &= \kappa_i E_i - (\gamma_i + \psi_i + \mu_i)I_i \\ \dot{R}_i &= \gamma_i I_i - (\tau_i + \mu_i)R_i \end{cases} \quad (8)$$

where $\tilde{p}_{kj} = \alpha_k p_{kj}$, $i = 1, 2, \dots, n$ and n is the number of patches.

For continuity, we present Table 7 which contains the definition of the parameters used in the model as is given in [1].

Parameters	Description
α_i	The proportion of individuals that leave their residence patch i
p_{ij}	The proportion of time that an individual from patch i spends in patch j , given that is one individual that leaves its residence patch
Λ_i	Recruitment of Susceptible individuals in Patch i
β_j	Instantaneous risk of infection in Patch j
μ_i	Per capita natural death rate in Patch i
γ_i	Per capita recovery rate of individuals in Patch i
τ_i	Per capita loss of immunity rate
ψ_i	Per capita disease induced death rate of Patch i
κ_i	Per capita rate at which the exposed individuals in patch i becomes infectious

Table 7: Description of the parameters.

To assess the role of mobility on the infection dynamics in the AGEBS in Hermosillo, we compare the effects of mobility changes for each period incorporating the estimated residence time matrices and the mobility parameter of each part into the epidemic model. The effect is evaluated by obtaining the difference between the two generated infection counts for $t \in (0, 200)$. The infection counts were obtained from mobility residence time matrices and mobility parameter vectors estimated (using the Brownian bridge technique as previously elaborated) within the calendar time periods described in Table 2. For instance, to measure the contribution of mobility in the evolution dynamics of the disease in the first period, we compute the difference between the infection counts generated by mobility residence time matrices and mobility parameter vectors in the FP_FP and FP_SP.

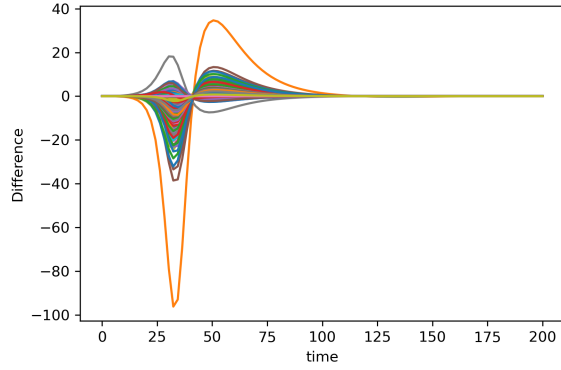
The epidemic parameters and initial state were fixed and all simulations and the number of initial infected individuals was determined from the observed Hermosillo COVID-19 infection data where there was one initial case each in four AGEBS with IDs 2956,

3367, 5734 and 6200. We therefore used, for the numerical simulation, the initial values: $E_{2956}(0) = E_{3367}(0) = E_{5734}(0) = E_{6200}(0) = 1$, $I_{2956}(0) = I_{3367}(0) = I_{5734}(0) = I_{6200}(0) = 1$, $E_i(0) = I_i(0) = 0$ for $i = \{1, 2, \dots, n\} \setminus \{2956, 3367, 5734, 6200\}$, $R_i(0) = 0$ and $S_i(0) = N_i - (E_i(0) + I_i(0) + R_i(0))$ for $i = 1, 2, \dots, n$. This scheme of initial values was chosen with the intention of ascertaining how mobility of the initial cases contributes to the evolution of the disease in all the AGEs in Hermosillo.

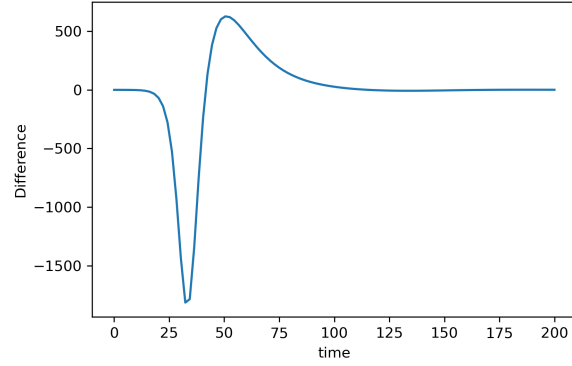
The demographic parameters used in the simulation were obtained from existing literature. [24] gives the crude death rate for the state of Sonora, Mexico as 6% of every 1000 persons per year. Since we are modelling the infection dynamics of individuals per day, we used a constant natural death rate of $\mu_i = \frac{0.06}{1000 \times 365}$ for each AGE. The population size, N_i , for each AGE was obtained from the 2019 Mexico census conducted by INEGI. Using the natural crude death rate and the population for each AGE (corresponding to each period and part), we obtained the recruitment rate of susceptibles for each AGE as $\Lambda_i = \mu_i N_i = \mu N_i$. Following [28] who postulated that the contact rate of COVID 19 is $\beta \in (0.5944, 1.68)$, we used $\beta_i = 1.5$ as the risk of infection in each AGE. Based on diverse literature on COVID 19, we used the incubation and recovery rates and the rate at which the recovered individuals become susceptible as $\kappa_i^{-1} = 7$ days, $\lambda_i^{-1} = 14$ days and $\tau_i^{-1} = 180$ days respectively.

Based on the difference between infection counts and proportions in each part, Figures 5, 6 and 7 shows that for each period, mobility had a role in the evolution of the disease both in individual AGEs and globally. For instance, it is clear from Figure 5A that for the first about $t = 30$ days, the disease evolved rapidly in most of the AGEs in the first period second part as compared to the first period first part. Thereafter, a faster evolution of the disease is observed in the first period first part as compared to first period second part. This observation is confirmed by Figure 5B which graphs the difference between the sum of the infection counts for each AGE in FP_FP and FP_SP at the time points. Similar observations can be made in Figures 6A and 6B and Figures 7A and 7B which are the plots of the differences in individual AGE and global infection counts for second period and third period respectively.

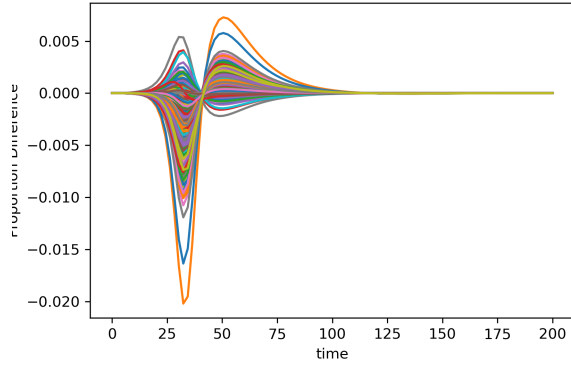
Figures 5C, 5D, 6C, 6D, 7C and 7D are plots of the difference in the normalized infection counts (proportions), both for individual AGEs and global, for the respectively indicated periods. Using the proportion differences, we still conclude that for all periods, the disease generally evolved faster in the second part for about the first 30 days, after which, there is an observed faster evolution of the disease in the first period. The evolution of the diseases in the second part was much faster in the first period followed by the third period and lastly, the second period. This can be observed from Figure 5A and 5C which shows larger magnitudes of the difference in the infection counts and proportions. Figure 7A and 7C confirms that the third period had the second largest count and proportion differences. However, the magnitude of the difference in the global infection counts and proportions in the first and third period appeared to be more or less of the same order. This can be



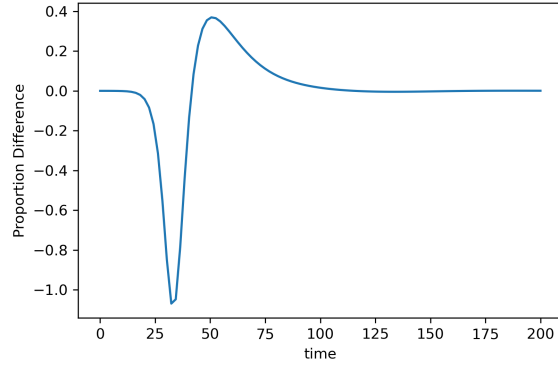
(A) Difference in individual AGEs infections in FP_FP and in FP_SP.



(B) Difference in global infections in FP_FP and in FP_SP.



(C) Difference in proportions of infections in individual AGEs in FP_FP and in FP_SP.

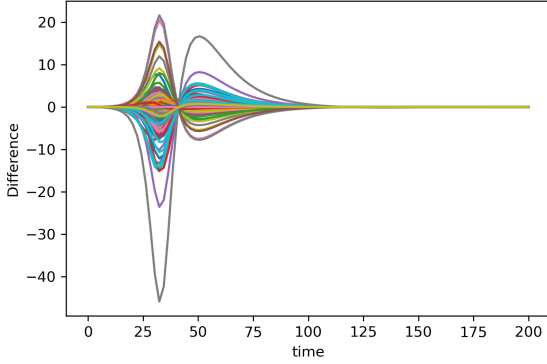


(D) Difference in proportions of global infections in FP_FP and in FP_SP.

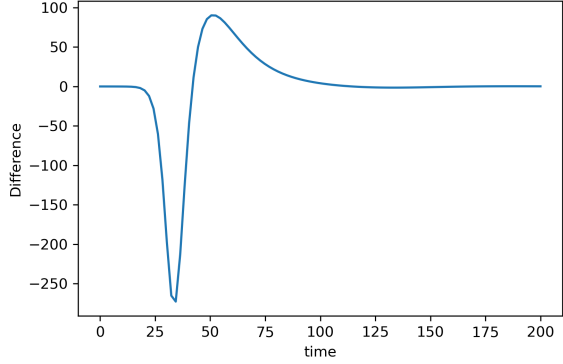
Figure 5: Differences in individual and global AGEs infection curves and proportions for First Period First Part and First Period Second Part.

confirmed from Figures 5D and 7D. We can thus posit that the speed of the the global evolution of the disease in the second part was the same in both the first and third periods.

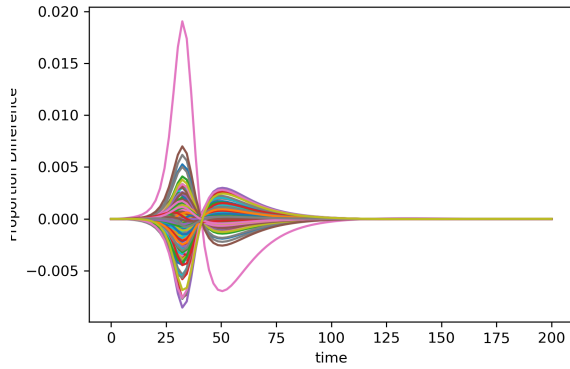
The previous results indicate that for each period, the mobility residence time matrices and mobility parameter vectors contributed to the change in infection levels for each corresponding part. More results can be conducted in this direction by considering statistical tests, for instance, but they are beyond the scope of this paper.



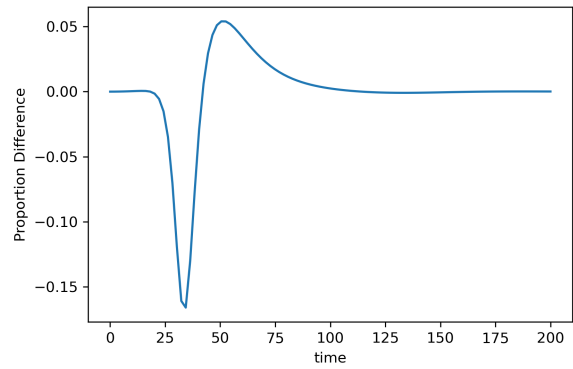
(A) Difference in individual AGEs infections in SP_FP and in SP_SP.



(B) Difference in global infections in SP_FP and in SP_SP.

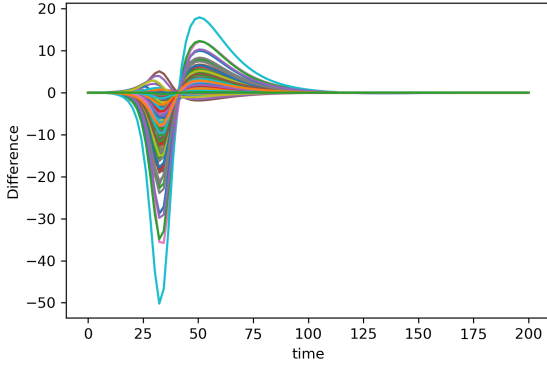


(C) Difference in proportions of infections in individual AGEs in SP_FP and in SP_SP.

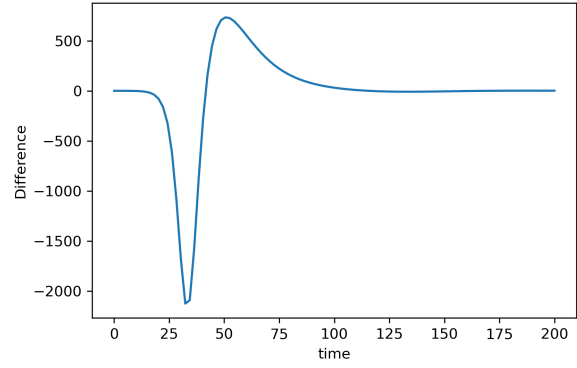


(D) Difference in proportions of global infections in SP_FP and in SP_SP.

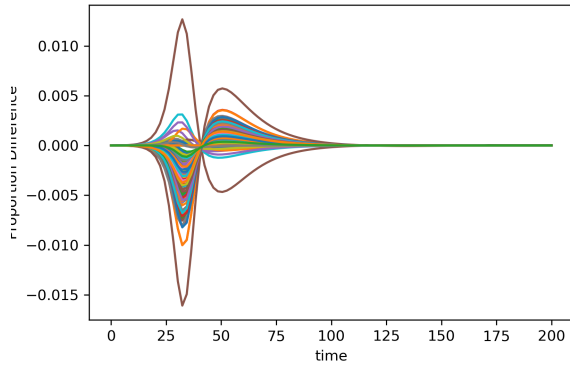
Figure 6: Differences in individual and global AGEs infection curves and proportions for Second Period First Part and Second Period Second Part.



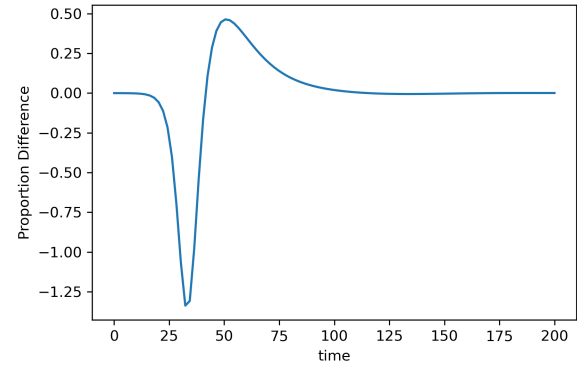
(A) Difference in individual AGEs infections in TP_FP and in TP_SP.



(B) Difference in global infections in TP_FP and in TP_SP.



(C) Difference in proportions of infections in individual AGEs in TP_FP and in TP_SP.



(D) Difference in proportions of global infections in TP_FP and in TP_SP.

Figure 7: Differences in individual and global AGEs infection curves and proportions for Third Period First Part and Third Period Second Part.

6 Conclusion

In this article, we propose a way to estimate characteristics of population mobility dynamics based on mobile phone data and Brownian-type stochastic models. Brownian bridges allow us to obtain a distribution of individual displacement trajectories, and with them, we can answer multiple mobility questions. In the application we estimate the residence and mobility matrix at the AGEb level that describes the mobility patterns for all the individuals that live in each AGEb.

Some of the challenges that persist in the use of mobile phone data for mobility analysis are the assumptions of representativeness of the sample and selection of AGEbs of residence. Thanks to the increasing use of smartphones, we consider that the database is a representative sample of the population. However, it is desirable to use descriptive and analytical techniques to compare with other sources of information to support the assumption that the sample has no important biases.

On the other hand, the selection of the AGEb of residence does not have an associated uncertainty. For a more detailed analysis, it is desirable to incorporate this in the matrix estimation. This matrix is an input for a multi-patch SEIR compartmental model. We provide new evidence on the real impact of population mobility on epidemiological evolution since we estimate the residence-mobility matrices utilizing actual data from the city of Hermosillo. The residence-mobility matrix and the alpha vector, which describes the proportion of people moving beyond their AGEb, are directly included in the multi-patch epidemiological model. A direct statistical estimation of all the parameters of the epidemiological model, including the residence-mobility matrix, is not very feasible since models with many parameters easily have identifiability problems.

Carrying out a study of scenarios or sensitivity of the epidemiological model may be desirable when the point estimate of the mobility and residence matrix is used as input. Still, techniques such as Bayesian can be explored to directly incorporate uncertainty in the epidemiological model.

Despite the improvements we can make, the mobility and its estimation, using mobile phone data, already allows generating important inputs to expand the scope of a many mathematical models that describe critical social phenomena such as the economy, violence, transmission of information or infectious diseases. With the proposed methodology, other estimates can also be made that consider, for example, mobility by time ranges, such as nighttime and weekends, or the description of mobility by subgroups, such as mobility by age groups and sex in the each area of interest.

7 Acknowledgment

This research has been funded by the CONTEX project 2020-93B Machine-Learning-Assisted Real-Time Simulations and Uncertainty Quantification for Infectious Disease Outbreaks.

References

- [1] A. O. AKUNO, L. L. RAMIREZ-RAMIREZ, C. MEHTA, C. KRISHNANUNI, T. BUI-THANH, AND J. A. MONTROYA, *Multi-patch epidemic models with partial mobility, residency, and demography*, preprint in Research Square, (2022). Available at <https://doi.org/10.21203/rs.3.rs-1954140/v1>.
- [2] K. AL-MAQRASHI, F. AL-MUSALHI, I. M. ELMOJTABA, AND N. AL-SALTI, *The impact of mobility between rural areas and forests on the spread of zika*, arXiv preprint arXiv:2108.11331, (2021).
- [3] J. ARINO AND P. VAN DEN DRIESSCHE, *A multi-city epidemic model*, Mathematical Population Studies, 10 (2003), pp. 175–193.
- [4] H. BARBOSA, M. BARTHELEMY, G. GHOSHAL, C. R. JAMES, M. LENORMAND, T. LOUAIL, R. MENEZES, J. J. RAMASCO, F. SIMINI, AND M. TOMASINI, *Human mobility: Models and applications*, Physics Reports, 734 (2018), pp. 1–74.
- [5] E. L. BERNARDO, T. NHAMPOSSA, K. CLOUSE, J. G. CARLUCCI, S. FERNÁNDEZ-LUIS, L. FUENTE-SORO, A. NHACOLO, M. SIDAT, D. NANICHE, AND T. D. MOON, *Patterns of mobility and its impact on retention in care among people living with hiv in the manhiça district, mozambique*, PloS one, 16 (2021), p. e0250844.
- [6] D. BICHARA AND A. IGGIDR, *Multi-patch and multi-group epidemic models: a new framework*, Journal of mathematical biology, 77 (2018), pp. 107–134.
- [7] D. BICHARA, Y. KANG, C. CASTILLO-CHAVEZ, R. HORAN, AND C. PERRINGS, *SIS and SIR epidemic models under virtual dispersal*, Bulletin of mathematical biology, 77 (2015), pp. 2004–2034.
- [8] V. D. BLONDEL, J.-L. GUILLAUME, R. LAMBIOTTE, AND E. LEFEBVRE, *Fast unfolding of communities in large networks*, Journal of statistical mechanics: theory and experiment, 2008 (2008), p. P10008.
- [9] F. CALABRESE, L. FERRARI, AND V. D. BLONDEL, *Urban sensing using mobile phone network data: a survey of research*, Acm computing surveys (csur), 47 (2014), pp. 1–20.

- [10] C. CASTILLO-CHAVEZ, D. BICHARA, AND B. R. MORIN, *Perspectives on the role of mobility, behavior, and time scales in the spread of diseases*, Proceedings of the National Academy of Sciences, 113 (2016), pp. 14582–14588.
- [11] S. CHANG, E. PIERSON, P. W. KOH, J. GERARDIN, B. REDBIRD, D. GRUSKY, AND J. LESKOVEC, *Mobility network models of covid-19 explain inequities and inform reopening*, Nature, 589 (2021), pp. 82–87.
- [12] V. COLIZZA, R. PASTOR-SATORRAS, AND A. VESPIGNANI, *Reaction–diffusion processes and metapopulation models in heterogeneous networks*, Nature Physics, 3 (2007), pp. 276–282.
- [13] W. COTA, D. SORIANO-PAÑOS, A. ARENAS, S. C. FERREIRA, AND J. GÓMEZ-GARDEÑES, *Infectious disease dynamics in metapopulations with heterogeneous transmission and recurrent mobility*, New Journal of Physics, 23 (2021), p. 073019.
- [14] G. M. DE SOUZA CONCEIÇÃO, G. L. BARBOSA, C. LORENZ, A. C. D. BOCEWICZ, L. M. R. SANTANA, C. C. DE AZEVEDO MARQUES, AND F. CHIARAVALLOTI-NETO, *Effect of social isolation in dengue cases in the state of sao paulo, brazil: an analysis during the covid-19 pandemic*, Travel medicine and infectious disease, 44 (2021), p. 102149.
- [15] P. V. DRIESSCHE, *Spatial structure: patch models*, in Mathematical epidemiology, Springer, 2008, pp. 179–189.
- [16] B. ESPINOZA, C. CASTILLO-CHAVEZ, AND C. PERRINGS, *Mobility restrictions for the control of epidemics: When do they work?*, Plos one, 15 (2020), p. e0235731.
- [17] S. FORTUNATO, *Community detection in graphs*, Physics reports, 486 (2010), pp. 75–174.
- [18] B. FURLETTI, L. GABRIELLI, F. GIANNOTTI, L. MILLI, M. NANNI, D. PEDRESCHI, R. VIVIO, AND G. GAROFALO, *Use of mobile phone data to estimate mobility flows. measuring urban population and inter-city mobility using big data in an integrated approach*, in Proceedings of the 47th Meeting of the Italian Statistical Society, 2014.
- [19] C. GARIAZZO AND A. PELLICIONI, *A multi-city urban population mobility study using mobile phone traffic data*, Applied Spatial Analysis and Policy, 12 (2019), pp. 753–771.
- [20] M. A. HERRERA-VALDEZ, M. CRUZ-APONTE, AND C. CASTILLO-CHAVEZ, *Multiple outbreaks for the same pandemic: Local transportation and social distancing explain the different “waves” of a-h1n1pdm cases observed in méxico during 2009*, Mathematical Biosciences & Engineering, 8 (2011), p. 21.
- [21] J. S. HORNE, E. O. GARTON, S. M. KRONE, AND J. S. LEWIS, *Analyzing animal movements using brownian bridges*, Ecology, 88 (2007), pp. 2354–2363.

- [22] K. KHAN, J. ARINO, W. HU, P. RAPOSO, J. SEARS, F. CALDERON, C. HEIDEBRECHT, M. MACDONALD, J. LIAUW, A. CHAN, ET AL., *Spread of a novel influenza a (h1n1) virus via global airline transportation*, New England journal of medicine, 361 (2009), pp. 212–214.
- [23] N. KISHORE, M. V. KIANG, K. ENGØ-MONSEN, N. VEMBAR, A. SCHROEDER, S. BALSARI, AND C. O. BUCKEE, *Measuring mobility to monitor travel and physical distancing interventions: a common framework for mobile phone data analysis*, The Lancet Digital Health, (2020).
- [24] KNOEMA, *World data atlas, mexico, sonora mortality*. <https://knoema.com/atlas/Mexico/Sonora/Crude-Death-Rate>, 2021.
- [25] J. KOOPMAN, *Modeling infection transmission*, Annu. Rev. Public Health, 25 (2004), pp. 303–326.
- [26] M. U. KRAEMER, N. GOLDING, D. BISANZIO, S. BHATT, D. M. PIGOTT, S. RAY, O. BRADY, J. BROWNSTEIN, N. FARIA, D. CUMMINGS, ET AL., *Utilizing general human movement models to predict the spread of emerging infectious diseases in resource poor settings*, Scientific reports, 9 (2019), pp. 1–11.
- [27] R. LAXMINARAYAN, B. WAHL, S. R. DUDALA, K. GOPAL, C. MOHAN B, S. NEELIMA, K. JAWAHAR REDDY, J. RADHAKRISHNAN, AND J. A. LEWNARD, *Epidemiology and transmission dynamics of covid-19 in two indian states*, Science, 370 (2020), pp. 691–697.
- [28] Q. LIN, S. ZHAO, D. GAO, Y. LOU, S. YANG, S. S. MUSA, M. H. WANG, Y. CAI, W. WANG, L. YANG, ET AL., *A conceptual model for the coronavirus disease 2019 (covid-19) outbreak in wuhan, china with individual reaction and governmental action*, International journal of infectious diseases, 93 (2020), pp. 211–216.
- [29] P. LIYANAGE, J. ROCKLÖV, AND H. A. TISSERA, *The impact of covid–19 lockdown on dengue transmission in sri lanka; a natural experiment for understanding the influence of human mobility*, PLoS neglected tropical diseases, 15 (2021), p. e0009420.
- [30] X. LU, L. BENGTSSON, AND P. HOLME, *Predictability of population displacement after the 2010 haiti earthquake*, Proceedings of the National Academy of Sciences, 109 (2012), pp. 11576–11581.
- [31] J. U. MÁRQUEZ URBINA, G. GONZÁLEZ FARÍAS, L. L. RAMÍREZ RAMÍREZ, AND D. I. RODRÍGUEZ GONZÁLEZ, *A multi-source global-local model for epidemic management*, Plos one, 17 (2022), p. e0261650.
- [32] J. M. MARSHALL, S. L. WU, H. M. SANCHEZ C, S. S. KIWARE, M. NDHLOVU, A. L. OUÉDRAOGO, M. B. TOURE, H. J. STURROCK, A. C. GHANI, AND N. M.

- FERGUSON, *Mathematical models of human mobility of relevance to malaria transmission in africa*, Scientific reports, 8 (2018), pp. 1–12.
- [33] M. G. MEEKAN, C. M. DUARTE, J. FERNÁNDEZ-GRACIA, M. THUMS, A. M. SEQUEIRA, R. HARCOURT, AND V. M. EGUÍLUZ, *The ecology of human mobility*, Trends in ecology & evolution, 32 (2017), pp. 198–210.
 - [34] V. MORENO, B. ESPINOZA, K. BARLEY, M. PAREDES, D. BICHARA, A. MUBAYI, AND C. CASTILLO-CHAVEZ, *The role of mobility and health disparities on the transmission dynamics of tuberculosis*, Theoretical Biology and Medical Modelling, 14 (2017), pp. 1–17.
 - [35] M. E. NEWMAN AND M. GIRVAN, *Finding and evaluating community structure in networks*, Physical review E, 69 (2004), p. 026113.
 - [36] T. NGUYEN AND B. K. SZYMANSKI, *Using location-based social networks to validate human mobility and relationships models*, in 2012 IEEE/ACM International Conference on Advances in Social Networks Analysis and Mining, IEEE, 2012, pp. 1215–1221.
 - [37] J. R. PALMER, T. J. ESPENSHADE, F. BARTUMEUS, C. Y. CHUNG, N. E. OZGENCIL, AND K. LI, *New approaches to human mobility: Using mobile phones for demographic research*, Demography, 50 (2013), pp. 1105–1128.
 - [38] F. PEÑUÑURI, J. MONTOYA, AND O. CARVENTE, *Density profiles of granular gases studied by molecular dynamics and brownian bridges*, Physica A: Statistical Mechanics and its Applications, 492 (2018), pp. 2103–2110.
 - [39] C. PERRINGS, C. CASTILLO-CHAVEZ, G. CHOWELL, P. DASZAK, E. P. FENICHEL, D. FINNOFF, R. D. HORAN, A. M. KILPATRICK, A. P. KINZIG, N. V. KUMINOFF, ET AL., *Merging economics and epidemiology to improve the prediction and management of infectious disease*, EcoHealth, 11 (2014), pp. 464–475.
 - [40] N. B. PONIEMAN, A. SALLES, AND C. SARRAUTE, *Human mobility and predictability enriched by social phenomena information*, in Proceedings of the 2013 IEEE/ACM International Conference on Advances in Social Networks Analysis and Mining, 2013, pp. 1331–1336.
 - [41] V. POZDNYAKOV, T. MEYER, Y.-B. WANG, AND J. YAN, *On modeling animal movements using brownian motion with measurement error*, Ecology, 95 (2014), pp. 247–253.
 - [42] P. PUCCI, F. MANFREDINI, AND P. TAGLIOLATO, *Mapping Urban Practices Through Mobile Phone Data*, SpringerBriefs in Applied Sciences and Technology, Springer International Publishing, 2015.

- [43] C. RATTI, D. FRENCHMAN, R. M. PULSELLI, AND S. WILLIAMS, *Mobile landscapes: using location data from cell phones for urban analysis*, Environment and planning B: Planning and design, 33 (2006), pp. 727–748.
- [44] Y. REN, *Appropriate population mobility management in an epidemic*, in COVID-19 and Cities, Springer, 2021, pp. 83–93.
- [45] A. RUIZ-HERRERA AND P. J. TORRES, *The role of movement patterns in epidemic models on complex networks*, Bulletin of mathematical biology, 83 (2021), pp. 1–13.
- [46] B. SAKAROVITCH, M.-P. D. BELLEFON, P. GIVORD, AND M. VANHOOF, *Estimating the residential population from mobile phone data, an initial exploration*, Economie et Statistique, 505 (2018), pp. 109–132.
- [47] A. F. SIEGENFELD AND Y. BAR-YAM, *The impact of travel and timing in eliminating covid-19*, Communications Physics, 3 (2020), pp. 1–8.
- [48] C. SONG, Z. QU, N. BLUMM, AND A.-L. BARABÁSI, *Limits of predictability in human mobility*, Science, 327 (2010), pp. 1018–1021.
- [49] D. SORIANO-PAÑOS, W. COTA, S. C. FERREIRA, G. GHOSHAL, A. ARENAS, AND J. GÓMEZ-GARDEÑES, *Modeling communicable diseases, human mobility, and epidemics: A review*, Annalen der Physik, (2022), p. 2100482.
- [50] M. TIZZONI, P. BAJARDI, A. DECUYPER, G. K. K. KING, C. M. SCHNEIDER, V. BLONDEL, Z. SMOREDA, M. C. GONZÁLEZ, AND V. COLIZZA, *On the use of human mobility proxies for modeling epidemics*, PLoS Comput Biol, 10 (2014), p. e1003716.
- [51] M. R. TOCTO-ERAZO, D. OLMOS-LICEAGA, AND J. A. MONTOYA, *Effect of daily periodic human movement on dengue dynamics: The case of the 2010 outbreak in Hermosillo, Mexico*, Applied Mathematical Modelling, 97 (2021), pp. 559–567.
- [52] V. A. TRAAG, L. WALTMAN, AND N. J. VAN ECK, *From louvain to leiden: guaranteeing well-connected communities*, Scientific reports, 9 (2019), pp. 1–12.
- [53] UN, *Un world urbanization prospects*, in UN World Urbanization Prospects, 2018.
- [54] B. WANG, M. GOU, Y. GUO, G. TANAKA, AND Y. HAN, *Network structure-based interventions on spatial spread of epidemics in metapopulation networks*, Physical Review E, 102 (2020), p. 062306.
- [55] D. WANG, D. PEDRESCHI, C. SONG, F. GIANNOTTI, AND A.-L. BARABASI, *Human mobility, social ties, and link prediction*, in Proceedings of the 17th ACM SIGKDD international conference on Knowledge discovery and data mining, 2011, pp. 1100–1108.

- [56] C. XIONG, S. HU, M. YANG, W. LUO, AND L. ZHANG, *Mobile device data reveal the dynamics in a positive relationship between human mobility and covid-19 infections*, Proceedings of the National Academy of Sciences, 117 (2020), pp. 27087–27089.
- [57] Y. YAN, A. A. MALIK, J. BAYHAM, E. P. FENICHEL, C. COUZENS, AND S. B. OMER, *Measuring voluntary and policy-induced social distancing behavior during the covid-19 pandemic*, Proceedings of the National Academy of Sciences, 118 (2021).
- [58] H. YILMAZKUDAY, *Stay-at-home works to fight against covid-19: International evidence from google mobility data*, Journal of Human Behavior in the Social Environment, 31 (2021), pp. 210–220.
- [59] Q. YIN, Z. WANG, C. XIA, M. DEHMER, F. EMMERT-STREIB, AND Z. JIN, *A novel epidemic model considering demographics and intercity commuting on complex dynamical networks*, Applied Mathematics and Computation, 386 (2020), p. 125517.
- [60] H. ZLOTNIK, *World urbanization: trends and prospects*, in New forms of urbanization, Routledge, 2017, pp. 43–64.